

# Electrostatics of surface-electrode ion traps

J. H. Wesenberg\*

*Department of Materials, University of Oxford, United Kingdom*

(Dated: December 18, 2008)

Surface-electrode (SE) rf traps are a promising approach to manufacturing complex ion-trap networks suitable for large-scale quantum information processing. In this paper we present analytical methods for modeling SE traps in the gapless plane approximation, and apply these methods to two particular classes of SE traps. For the SE ring trap we derive analytical expressions for the trap geometry and strength, and also calculate the depth in the absence of control fields. For translationally symmetric multipole configurations (analogs of the linear Paul trap), we derive analytical expressions for electrode geometry and strength. Further, we provide arbitrarily good approximations of the trap depth in the absence of static fields and identify the requirements for obtaining maximal depth. Lastly, we show that the depth of SE multipoles can be greatly influenced by control fields.

PACS numbers: 37.10.Gh, 41.20.Cv

Several approaches to large-scale quantum information processing (QIP) with trapped ions using networks of interconnected rf traps have been proposed [1, 2, 3]. Surface-electrode (SE) ion traps, where the trap electrodes are located in a single plane as illustrated in Fig. 1, offer a promising approach to constructing such trap networks [4, 5, 6]. SE traps are well suited for microfabrication, and motional heating rates compatible with QIP have been demonstrated [5, 6], an important fact since motional heating is currently a limiting factor for ion-trap miniaturization [7, 8].

Except for analytical results for some high symmetry configurations [9], modeling of SE traps has so far been based mostly on numerical techniques. While this approach is feasible for modeling with the purpose of characterizing the trap provided by a given electrode structure, it is inconvenient for modeling with the purpose of designing traps to best meet design criteria. This is unlike the situation in traditional rf traps such as the linear Paul trap [10], where the electrodes surround the ion, and where symmetry considerations together with scaling relations often provide sufficient background for trap design.

In this paper, we present two methods for the design of SE traps. Firstly, we demonstrate that a relatively unknown technique makes it possible to analytically calculate the field resulting from an arbitrary configuration of surface electrodes in the “gapless plane” approximation where the electrodes are assumed to gaplessly cover an infinite plane. Secondly, we show that the important case of multipole guides with translationally symmetric electrode configurations (analogs to the linear Paul trap), can be given a simple geometrical description through a conformal map. Together with recent results on the fundamental constraints on intersections in rf trap networks [11], the results presented here can serve as guidelines in the design and modeling of SE ion trap networks.

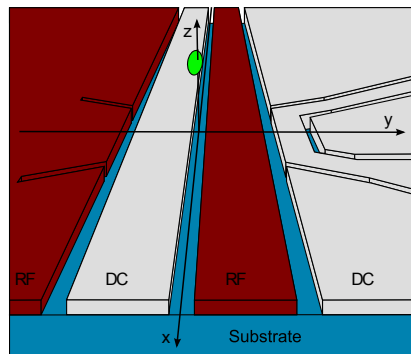


FIG. 1: (Color online) Cut near the trap center (oval) of a surface-electrode (SE) trap, showing the rf and control (DC) electrodes on an insulating substrate. Design, including the aspect ratio of the gaps between electrodes, corresponds roughly to that of the trap described in Ref. [5], for an ion surface distance of  $40\ \mu\text{m}$ . The electrodes extend beyond the illustrated area in all directions.

The paper is structured as follows: Sec. I introduces the fundamental task of ion-trap modeling. In Sec. II, we argue that SE traps can be modeled as an infinite plane gaplessly covered by electrodes and describe an analytical method for calculating the field of arbitrarily shaped surface electrodes in this approximation. In Sec. III we apply this method to the analysis of the SE ring trap. Sections IV and V are devoted to parametrizing and analyzing translationally symmetric SE configurations.

## I. RF ION TRAPS FOR QIP

In this section we introduce the basic physics of rf traps and the role of electrostatic modeling in the characterization of such traps.

For the typical dimensions ( $\mu\text{m}$ ) and rf frequencies (MHz) of the rf traps typically used for QIP, the rf field can be adequately treated as quasistatic [12]. Following Ref. [13] we introduce the electrode basis function

\*janus.wesenberg@materials.ox.ac.uk

$\Theta_\gamma(\mathbf{r})$  for an electrode  $\gamma$  as the unique function that takes the value 1 (0) for  $\mathbf{r}$  on the surface of electrode  $\gamma$  (all other electrodes) and fulfills the Laplace condition  $\nabla^2\Theta_\gamma(\mathbf{r}) = 0$ . In terms of the electrode basis functions, the spatial potential obtained by applying a voltage  $V_\gamma$  to electrode  $\gamma$  while keeping all other electrodes grounded is  $\bar{V}_\gamma(\mathbf{r}) \equiv V_\gamma\Theta_\gamma(\mathbf{r})$ . Neglecting any nonlinear electric properties of the trap materials, the total field  $\mathbf{E}_{\text{Tot}}(\mathbf{r})$  in the trap can be expressed as

$$\mathbf{E}_{\text{Tot}}(\mathbf{r}, t) = -(V_{\text{rf}} \cos(\Omega t) + V_{c,\text{rf}}) \nabla\Theta_{\text{rf}}(\mathbf{r}) - \sum_i V_{c,i} \nabla\Theta_{c,i}(\mathbf{r}),$$

where  $\Omega$  is the rf frequency,  $V_{\text{rf}}$  is the peak rf voltage,  $V_{c,\text{rf}}$  is the bias applied to the rf electrodes, and  $V_{c,i}$  is the voltage applied to control electrode  $i$ . In most applications the applied voltages will be modified quasistatically to manipulate the trap, but we shall not be concerned with this in what follows. To maintain physical dimensions, we will express most results in terms of the spatial potential  $\bar{V}_\gamma(\mathbf{r})$  and the corresponding field  $\mathbf{E}_\gamma(\mathbf{r}) \equiv -\nabla\bar{V}_\gamma(\mathbf{r})$ . Note that with this convention  $\mathbf{E}_{\text{rf}}$  is the rf field amplitude rather than the instantaneous rf field.

In an rf trap, the rf period  $2\pi/\Omega$  is made to be the shortest timescale of the system, so that in the adiabatic approximation the effect of the rf field on an ion of charge  $Q$  and mass  $M$  is described by the ponderomotive potential

$$U_p(\mathbf{r}) \equiv \frac{Q^2}{4M\Omega^2} |\mathbf{E}_{\text{rf}}(\mathbf{r})|^2, \quad (1)$$

corresponding to the kinetic energy of the micromotion induced by the rf field [14, 15]. Including the effects of the quasistatic control fields, the effective external potential experienced by a trapped ion is

$$U_{\text{eff}}(\mathbf{r}) \equiv U_p(\mathbf{r}) + Q \left[ \bar{V}_{c,\text{rf}}(\mathbf{r}) + \sum_i \bar{V}_{c,i}(\mathbf{r}) \right]. \quad (2)$$

Although trapping at the local minima of  $U_{\text{eff}}$  where  $U_p$  is non-zero is possible, it is usually avoided as the micromotion associated with a non-zero rf field amplitude can have a range of detrimental effects. In the following, we will only consider trapping at points where  $\mathbf{E}_{\text{rf}}(\mathbf{r}) = \mathbf{0}$ .

## II. FIELD OF ARBITRARY SURFACE ELECTRODES

In the following, we argue that it is in many cases reasonable to model an SE trap as an infinite plane gaplessly covered by electrodes. Further, we show that in this approximation the field of an arbitrary electrode can be calculated analytically. Lastly, we consider the field in terms of the Fourier components of the electrode shapes.

### A. Gapless plane approximation

As introduced above, an SE trap has all electrodes located in a single plane, typically on the surface of an insulating substrate as illustrated in Fig. 1 [4, 5, 6].

We will model the SE configuration in the gapless plane approximation, where the gaps between individual electrodes are assumed to be infinitely small and the electrodes are assumed to fully cover an infinite plane with no other conductors above the plane. It is clear that with  $d$  denoting the ion-electrode distance, necessary conditions for the gapless plane approximation to be valid include that gaps between electrodes are much smaller than  $d$ , that the extend of the trap is much larger than  $d$ , and that the distance from ion to other conducting surfaces is much larger than  $d$ .

These requirements are often met in SE traps. Firstly, although small electrode gaps lead to high field gradients, SE traps are usually constructed with small inter-electrode gaps since any exposed surface of the substrate would be prone to pick up static charges disturbing the operation of the trap. The condition on the absence of other conductors in the trap region imposes constraints on the experimental apparatus, but will in many cases be met. The corrections due to nearby conductors will be first order in the ratio of the total electrode extend to the distance to the conductors. For larger trap arrays, this could be a significant effect and corrections should ideally be made.

In the gapless plane approximation, the electrostatic modeling for a patch electrode  $\gamma$ , covering a region  $A_\gamma$  of the electrode plane reduces to identifying the unique potential  $\bar{V}_\gamma(\mathbf{r})$  so that  $\nabla^2\bar{V}_\gamma(\mathbf{r}) = 0$  and

$$\bar{V}_\gamma(x, y, 0) = \begin{cases} V_\gamma & \text{for } (x, y) \in A_\gamma \\ 0 & \text{otherwise,} \end{cases} \quad (3)$$

where we have chosen the  $x$ - $y$  plane to coincide with the electrode plane.

### B. Biot-Savart law

As shown in Ref. [16], the electrical potential  $\bar{V}_\gamma(\mathbf{r})$  satisfying the boundary condition of Eq. (3) can be very elegantly expressed in terms of the solid angle  $\Omega_{A_\gamma}(\mathbf{r})$  spanned by  $A_\gamma$  as seen from  $\mathbf{r}$ ,

$$\bar{V}_\gamma(\mathbf{r}) = V_\gamma \frac{\Omega_{A_\gamma}(\mathbf{r})}{2\pi}. \quad (4)$$

Taking the electrode plane to be the  $x$ - $y$  plane, and assuming  $z > 0$ , we have that

$$\Omega_A(\mathbf{r}) = \int_A \frac{(\mathbf{r} - \mathbf{r}') \cdot \hat{\mathbf{z}}}{|\mathbf{r} - \mathbf{r}'|^3} dx' dy'.$$

The corresponding field takes the form [16]

$$\mathbf{E}_\gamma(\mathbf{r}) = \frac{V_\gamma}{2\pi} \oint_{\partial A_\gamma} \frac{d\mathbf{r}' \times (\mathbf{r} - \mathbf{r}')}{|\mathbf{r} - \mathbf{r}'|^3}, \quad (5)$$

where the integral is counterclockwise (as seen from above) along the edge  $\partial A_\gamma$  of  $A_\gamma$ . Note that the integral is a Biot-Savart integral, so that  $\mathbf{E}_\gamma$  is proportional to the magnetic field that would be observed if a current was run along a wire following the edge of  $A_\gamma$ . This points to a close connection to work on “atom chips” using microfabricated wires [17, 18, 19], but it should be noted that this system is fundamentally different since magnetostatic traps can trap at nonzero field minima without adverse effects. Numerical integration of Eq. (5) can benefit from the results of Ref. [20].

### C. Fourier description of SE fields

For some applications, e.g. trap arrays [21], it is useful to describe the surface electrodes in terms of their Fourier transforms [22]. This approach also provides insight into the  $z$  dependence of SE fields in general.

By employing the Dirichlet Green’s function also used in Ref. [16], we find that in terms of  $\mathbf{k} \equiv k_x \hat{\mathbf{x}} + k_y \hat{\mathbf{y}}$  the Fourier transform  $\tilde{V}(\mathbf{k}, z) \equiv \int e^{-i\mathbf{k}\cdot\mathbf{r}} \tilde{V}(\mathbf{r}) dx dy$  of  $\tilde{V}(x, y, z)$  with respect to the  $x$  and  $y$  coordinates for a constant  $z$  value is given in terms of the surface potential  $\tilde{V}_{\text{surf}}(x, y) \equiv \tilde{V}(x, y, 0)$  by

$$\begin{aligned} \tilde{V}(\mathbf{k}, z) &= \int e^{-i\mathbf{k}\cdot\mathbf{r}} \frac{1}{2\pi} \frac{|\hat{\mathbf{z}}\cdot\mathbf{r}|}{|\mathbf{r}-\mathbf{r}'|^3} \tilde{V}_{\text{surf}}(x', y') dx dy dx' dy' \\ &= e^{-k|z|} \tilde{V}_{\text{surf}}(\mathbf{k}), \end{aligned} \quad (6)$$

where  $\tilde{V}_{\text{surf}}(\mathbf{k}) \equiv \int e^{-i\mathbf{k}\cdot\mathbf{r}} V_{\text{surf}}(x, y) dx dy$  is the Fourier transform of  $V_{\text{surf}}$ . Equation (6) implies that the Fourier components of  $V$  at a given  $z$  value fall off exponentially with  $z$  on the length scale of the electrode dimensions.

For our purpose,  $\tilde{V}_{\text{surf}}$  will be equal to  $V$  on some region  $A$  and zero elsewhere. In this case,  $\tilde{V}_{\text{surf}}$  can be calculated by noting that since  $e^{-i\mathbf{k}\cdot\mathbf{r}}$  is equal to the  $z$  component of the curl of the vector field  $\frac{i}{k^2} (\hat{\mathbf{z}} \times e^{-i\mathbf{k}\cdot\mathbf{r}} \mathbf{k})$  and the vector triple product  $\mathbf{a} \times \mathbf{b} \cdot \mathbf{c}$  is invariant under cyclic permutations, the Fourier transform can be converted to the path integral

$$\tilde{V}_{\text{surf}}(\mathbf{k}) = V \frac{i}{k^2} \hat{\mathbf{z}} \cdot \oint_{\partial A} e^{-i\mathbf{k}\cdot\mathbf{r}} \mathbf{k} \times d\mathbf{r},$$

where the integral is counterclockwise along the edge ( $\partial A$ ) of  $A$ .

## III. RING TRAP

To illustrate the application of the electrostatic methods presented in the previous section to rf trap analysis, we will, as an example, consider the SE version of a quadrupole ring trap [10]. We will show below that this can be implemented as a single ring-shaped rf electrode with inner and outer radii  $R_1$  and  $R_2$ , as illustrated by Fig. 2.

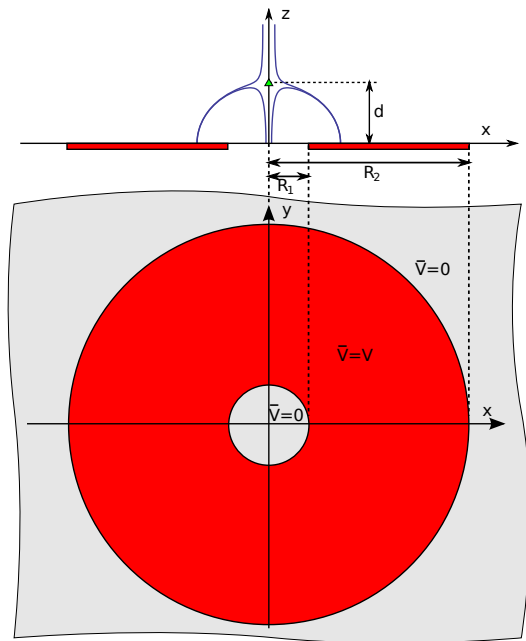


FIG. 2: (Color online) Strongest possible SE ring-trap configuration. Upper part: Cut plane through the rotational symmetry ( $z$ ) axis, together with the trap center (triangle) at a distance  $d$  above the electrode plane, cut of ring electrode (rectangles below the  $x$  axis), and field lines. Lower part: Top view of the electrode ( $x$ - $y$ ) plane, which in the gapless plane model is assumed to be grounded everywhere but on the ring electrode with inner (outer) radius  $R_1$  ( $R_2$ ).

The field of the ring electrode at potential  $V$  can be calculated as the superposition of the fields of a disk of radius  $R_2$  at potential  $V$  and a disk of radius  $R_1$  at potential  $-V$ , so that the combined field is  $\mathbf{E} \equiv \mathbf{E}_{R_2} - \mathbf{E}_{R_1}$ , where  $\mathbf{E}_R$  is the field of a disk of radius  $R$  at potential  $V$ . By symmetry, the electric field on the  $z$  axis must be aligned along the axis, and by Eq. (4) we find that

$$\mathbf{E}_R(z \hat{\mathbf{z}}) = V \frac{R^2}{(R^2 + z^2)^{3/2}} \hat{\mathbf{z}}. \quad (7)$$

See, e.g., [23] for the off-axis case.

For certain values of  $R_1$  and  $R_2$ , we find that  $E_z(z \hat{\mathbf{z}})$  vanishes for some value of  $z$ . When rf is applied to the ring electrode, such zeros correspond to points of zero rf field amplitude, which provide an ideal trapping point as discussed in Sec. I.

Rather than trying to determine the position of any field zeros for given dimensions of the ring electrode, we will consider the constructive design problem of parametrizing all values of  $R_1$  and  $R_2$  so that a field zero is located at a chosen distance  $d$  above the electrode plane. As an intermediate step to achieving this,

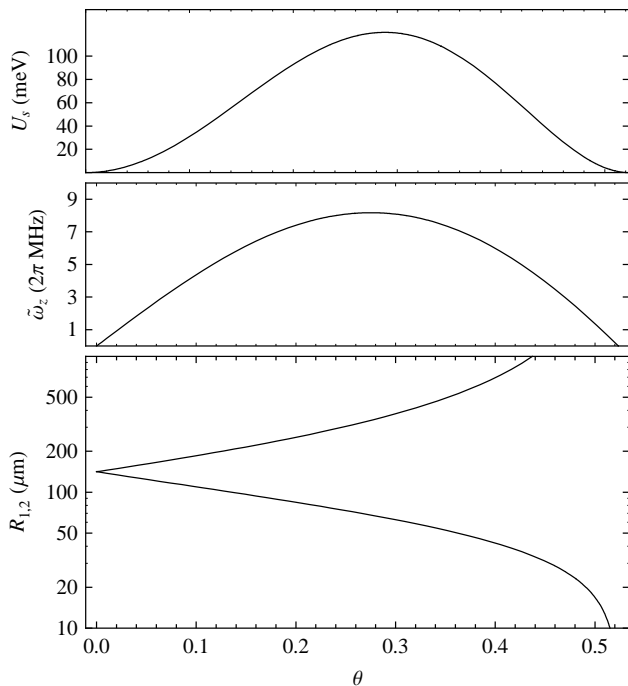


FIG. 3: Properties of the SE ring trap as a function of the parameter  $\theta$  appearing in Eq. (8) for the example parameter values given in Eq. (11).  $U_s$  (top) is the value of  $U_{\text{eff}}$  at the saddle position in the absence of any control fields.  $\tilde{\omega}_z \equiv q_z \Omega / \sqrt{8}$  (middle) is the adiabatic approximation of  $\omega_z$ , valid when  $q_z \ll 1$ .  $R_{1,2}$  (bottom) are the inner and outer radii of the ring electrode. The strongest trap is obtained for  $\theta \approx 0.275$ , where  $\tilde{\omega}_z \approx 2\pi \times 8.17$  MHz,  $U_s \approx 118$  meV, and  $R_{1,2} \approx \{68, 338\} \mu\text{m}$ . Scaling of  $q_z$ ,  $U_s$ , and  $R_{1,2}$  are given by Eqs. (9), (12), and  $d$ , respectively.

we parametrize  $R_i$  as  $d \tan(\phi_i)$  so that

$$E_z(d\hat{z}) = \frac{V}{d} \left( \cos(\phi_1) [1 - \cos^2(\phi_1)] - \cos(\phi_2) [1 - \cos^2(\phi_2)] \right).$$

For  $E_z(d\hat{z})$  to vanish,  $\cos(\phi_1)$  and  $\cos(\phi_2)$  must be roots of the polynomial  $u(1 - u^2) - a$  for some common constant  $a$ . This polynomial equation is in the Vieta standard form [24], and the solutions of interest to us can be parametrized as  $\cos(\phi_{1,2}) = 2 \sin(\pi/6 \pm \theta) / \sqrt{3}$ , corresponding to  $R$  values of

$$R_{1,2} = d \sqrt{\frac{3}{4} \sin^{-2} \left( \frac{\pi}{6} \pm \theta \right) - 1}, \quad 0 < \theta < \frac{\pi}{6}. \quad (8)$$

This, in particular, implies that the smallest outer radius of the ring electrode is  $R_2 = d\sqrt{2}$ .

#### A. Ring -trap characteristics

The different values of the parameter  $\theta$  appearing in Eq. (8) lead to traps with different properties. In the

following we consider the strength and the depth of the trap, as illustrated in Fig. 3.

The strength of an rf quadrupole trap is usually described by the dimensionless parameter  $q_z$  defined as [14]

$$q_z \equiv q_0 \left| \frac{1}{2} \frac{\partial^2 \bar{V}_{\text{rf}}(\mathbf{r})}{\partial z^2} \right| \left( \frac{V_{\text{rf}}}{d^2} \right)^{-1}, \quad q_0 \equiv \frac{4V_{\text{rf}}Q}{M\Omega^2 d^2}, \quad (9)$$

where  $q_0$  has the same scaling properties as  $q_z$ . In the adiabatic limit where the ponderomotive approximation is valid, the secular oscillation frequency  $\omega_z$  in the  $z$  direction is seen from Eq. (2) to be  $q_z \Omega / \sqrt{8}$ .

For the ring trap the rotational symmetry and the Laplace condition imply that the lowest-order multipole contributing at the field zero must be a quadrupole term of the form  $\mathbf{E}(\mathbf{r}) = -\alpha_z^{(2)} (2z\hat{z} - x\hat{x} - y\hat{y}) + \mathcal{O}(\mathbf{r}^2)$ . The quadrupole strength  $\alpha_z^{(2)}$  can be calculated as  $\alpha_z^{(2)} = -\frac{1}{2} (\partial E_z / \partial z)$ . Evaluating the derivative of  $\mathbf{E}_{R_2} - \mathbf{E}_{R_1}$  according to Eq. (7), we can write the resulting strength  $q_z = q_0 |\alpha_z^{(2)}| d^2 / V$  explicitly in terms of the parameter  $\theta$ .

$$q_z = q_0 \frac{1}{3} [\sin(5\theta) - \sin(\theta)], \quad (10)$$

which reaches a maximum value of  $q_z \approx 0.473 q_0$  when  $\cos^2(\theta) = (25 + \sqrt{145})/40$ . For typical parameters of

$$\Omega = 2\pi \times 100 \text{ MHz}, \quad V_{\text{rf}} = 100 \text{ V}, \quad (11a)$$

$$M = 10 \text{ AMU}, \quad d = 100 \mu\text{m}, \quad (11b)$$

we find that  $q_0 = 0.98$ .

In addition to the trap strength, it is of practical interest to know the depth of the trap, that is, the minimal energy required for a trapped ion to escape. To establish the depth we assume that the amplitude of the micromotion induced by the rf field is small compared with the dimensions of the potential. In this case, the depth of the trap region corresponds to the height of the (lowest) saddle point,  $\mathbf{r}_s$ , of the trapping (local) minima of  $U_{\text{eff}}$ . We will for now ignore the control-field contributions to  $U_{\text{eff}}$ , and only consider the ‘‘intrinsic depth,’’  $U_s \equiv U_p(\mathbf{r}_s)$  provided by the ponderomotive potential of the rf field. By Eq. (1),  $U_s$  is equal to

$$U_s \equiv U_0 \left| \frac{\mathbf{E}_{\text{rf}}(\mathbf{r}_s)}{V_{\text{rf}}/d} \right|^2, \quad U_0 \equiv \frac{Q^2 V_{\text{rf}}^2}{4M\Omega^2 d^2}, \quad (12)$$

where  $U_0$  has the scaling properties of the depth. As we shall see by example in Sec. VB, control fields can significantly change the effective depth of SE traps.

For the example parameters of Eq. (11),  $U_0 = 6.1$  eV, which is not a typical depth: as illustrated by Fig. 3 the maximal obtainable depth for a ring trap corresponds to less than 2% of  $U_0$ .

#### IV. SE MULTIPOLES

Linear rf traps, such as the linear Paul trap, are based on an rf multipole field, which is translationally invariant

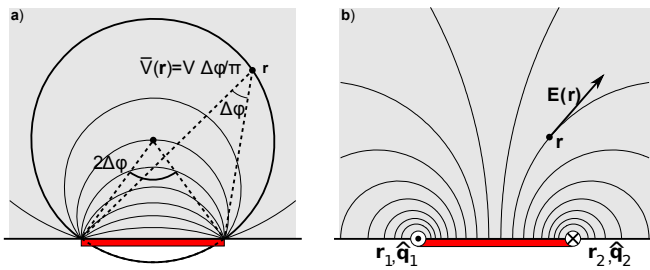


FIG. 4: (Color online) The potential (a) and field (b) above a strip electrode at potential  $V$  (rectangle) with edges at  $\mathbf{r}_1$  and  $\mathbf{r}_2$  in an infinite grounded plane. (a) Since the solid angle spanned by the strip is  $\Omega = 2\Delta\phi$ , it follows from Eq. (4) that the equipotential lines are circular arcs through the strip edges as discussed in the text. (b) By Eq. (5), the field is proportional to the magnetic field that would result from running a current along the edges of the strip in directions  $\hat{\mathbf{q}}_{1,2}$ .  $\mathbf{E}(\mathbf{r})$  is given algebraically by Eq. (13). The field (potential) can be compactly expressed as a complex Pólya field (complex-valued potential) according to Eqs. (16) and (17).

along the trap axis thus providing a multipole guide. In addition to the ponderomotive potential provided by the rf field, quasistatic control fields are used to control the total trapping potential as illustrated in Fig. 1. With 3D electrode structures, the multipole guide can typically be designed by symmetry considerations alone. In the linear Paul trap, four parallel electrodes are used, an approach which can be extended to higher-order multipoles [14]. The same symmetry considerations are not applicable to surface-electrode traps where only a few configurations of high symmetry have been analyzed [4, 9].

In the following, we aim to present a simple geometric theory of multipole guides in SE traps, as well as analytical methods for calculating the field in general translationally symmetric electrode configurations. The program will be similar to that followed in Sec. III for the ring trap: We will first introduce a constructive parametrization of all possible SE multipoles with a specific center position, and subsequently analyze trapping strength and depth in terms of the design parameters. In this case we will also briefly discuss the effects of biasing the rf electrodes.

### A. Pólya field

In the remainder of the paper, we will orient the coordinate system so that the translational symmetry is along the  $z$  axis and the electrode plane is parallel to the  $y$  axis at  $x = d$ . In figures we will orient the coordinate system so that the origin (trap center) is above the electrode plane, i.e., with the  $x$  axis pointing downward.

It follows from Eq. (5) that the field of a strip electrode with edges intersecting the  $x$ - $y$  plane in  $\mathbf{r}_1$  and  $\mathbf{r}_2$  is given

by

$$\mathbf{E}(\mathbf{r}) = \frac{V}{\pi} \sum_{i=1}^2 \frac{\hat{\mathbf{q}}_i \times (\mathbf{r} - \mathbf{r}_i)}{|\mathbf{r} - \mathbf{r}_i|^2}, \quad (13)$$

for  $\mathbf{r}$  in the trap region where  $\hat{\mathbf{q}}$  is  $\hat{\mathbf{z}}$  ( $-\hat{\mathbf{z}}$ ) for the left (right) edge as illustrated in Fig. 4(b). In terms of the azimuthal angle  $\Delta\phi$  spanned by the strip electrode as seen from  $\mathbf{r}$ , the solid angle spanned by the electrode is  $\Omega = 2\Delta\phi$  so that by Eq. (4)  $\bar{V}(\mathbf{r}) = V\Delta\phi/\pi$ . This, in particular, implies that the equipotential lines are circles through  $\mathbf{r}_1$  and  $\mathbf{r}_2$  as illustrated in Fig. 4(a).

Although compact, the vector nature of Eq. (13) leads to somewhat unwieldy expressions for the combined field of several strip electrodes. A simpler representation can be obtained by mapping the point  $\mathbf{r}$  in the  $x$ - $y$  plane to the complex point  $p$ ,

$$p(\mathbf{r}) \equiv x + iy, \quad (14)$$

and the vector field  $\mathbf{E}(\mathbf{r})$  to the complex function

$$\tilde{E}(p) \equiv E_x(\mathbf{r}(p)) + i E_y(\mathbf{r}(p)). \quad (15)$$

As discussed in more detail in Appendix B,  $\mathbf{E}$  is the Pólya field of  $\tilde{E}^*$  and  $\tilde{E}^*(p)$  is an analytical function of  $p$  if and only if  $\mathbf{E}$  is a divergence-free and irrotational vector field.

In terms of  $\tilde{E}$ , the field of a strip electrode as given by Eq. (13) is

$$\tilde{E}^*(z) = \frac{V}{i\pi} \sum_{i=1}^2 \frac{q_i}{z - z_i}, \quad (16)$$

where  $z = p(\mathbf{r})$ ,  $z_i = p(\mathbf{r}_i)$ , and  $q_i \equiv \hat{\mathbf{q}}_i \cdot \hat{\mathbf{z}}$ . We have expressed  $\tilde{E}^*$  in terms of  $z$  rather than  $p$  because it turns out that Eq. (16) as well as Eq. (17) below hold without any modification for the boundary conditions of a grounded cylinder ( $z = c$ ) as we shall see in the next section.

The complex potential  $\Phi(z)$  fulfilling  $\tilde{E}^*(z) = -\partial\Phi(z)/\partial z$  is given by

$$\Phi(z) = V \frac{i}{\pi} \sum_{i=1}^2 q_i \ln(z - z_i), \quad (17)$$

up to a complex constant. The real-valued physical potential  $\bar{V}$  is equal to the real part of  $\Phi$  as discussed in Appendix B. For the purpose of calculating derivatives Eq. (17) is valid as it stands, but care should be taken to choose the branch cut for the logarithm to ensure continuity if the value of  $\Phi$  is to be calculated directly.

### B. Parametrization of SE multipoles

With the Pólya field description of strip electrode fields provided by Eqs. (16) and (17), identifying the field zeros, i.e., trapping points, for a set of  $n$  strip electrodes is

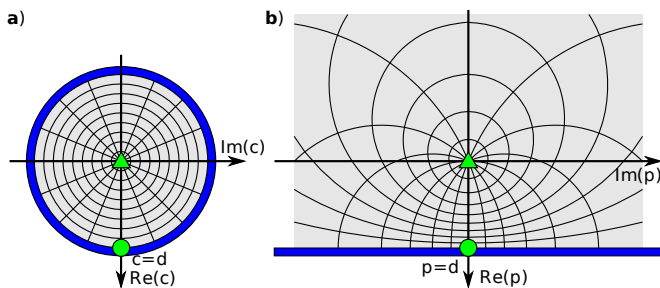


FIG. 5: (Color online) A graphical representation of the conformal map  $c \rightarrow p(c)$  mapping the inside of a conducting cylinder to the trapping region above an infinite conducting plane, as defined formally by Eq. (18). Green circles and triangles indicate the fixpoints at the point on the electrode plane right below the trap center ( $c = p = d$ ) and at the trap center ( $c = p = 0$ ), respectively. Thick blue lines indicate the electrode surface in the cylinder picture (a) and the SE picture (b).

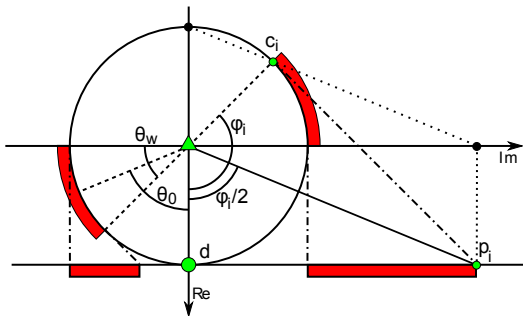


FIG. 6: (Color online) Parametrization of multipole electrodes and geometrical implementation of the map Eq. (18) for the electrode surface. The plot shows the electrodes in the  $c$  and  $p$  representation superimposed. Electrode positions for SE multipoles are specified by the parameters  $n$ ,  $\theta_0$ , and  $\theta_w$  according to Eq. (20). The example configuration corresponds to that of Fig. 7(b). An arbitrary point  $c_i = d \exp(i\phi_i)$  on the electrode plane of the cylinder is mapped to  $p_i = p(c_i)$  on the SE electrode plane  $\text{Re}(p) = d$  according to Eqs. (18) or (19). The mapping can be performed geometrically by extending the circle tangent at  $c_i$  to the line  $\text{Re}(p) = d$  (dash-dotted), or by a Mercator projection to the imaginary axis (dotted).

reduced to the problem of finding the roots of a polynomial of order  $2n - 1$ . Similarly, the task of characterizing the identified trapping points in terms of multipole coefficients is reduced to series expansion as discussed in Appendix B.

Although this can be achieved in many cases, we are often interested in the inverse problem: how to place strip electrodes to achieve a multipole guide of certain strength and orientation, and how these parameters relate to total electrode area and other implementation considerations. To solve this, it is convenient to map the trapping region conformally to a cylinder centered at the desired guide center, as an arbitrary multipole in a cylinder with conducting walls can be designed by symmetry consider-

ations alone as detailed below.

We choose the trap center as the origin at a distance  $d$  from the electrode plane given by  $x = d$ , or equivalently,  $\text{Re}(p) = d$ , as illustrated in Fig. 5. A conformal map which maps the cylinder  $|c| = d$  to the electrode plane  $\text{Re}(p) = d$  with fixpoints at  $c=p=0$  (trap center) and  $c=p=d$  (point on the electrode plane below the trap center) is given by the conformal (Möbius) map

$$p(c) \equiv d \frac{2c}{d+c}, \quad (18)$$

as illustrated in Fig. 5.

For the purpose of trap design, we are mostly concerned with the mapping of the electrode structure. Here, we find that a point  $c = d \exp(i\phi)$  on the cylinder surface is mapped to

$$\mathbf{r}(p(d e^{i\phi})) = d \hat{\mathbf{x}} + d \tan\left(\frac{\phi}{2}\right) \hat{\mathbf{y}}, \quad (19)$$

with a simple geometrical interpretation as illustrated in Fig. 6.

For the purpose of characterizing the SE multipoles, we will introduce a parametrization of the simplest possible multipole guides where an  $n$ th-order guide is implemented with  $n$  strip electrodes placed equidistantly around the cylinder walls. We will parametrize this configuration by the angle of  $\theta_w$  spanned by each strip as seen from the cylinder center, and the azimuthal angle  $\theta_0$  of the center of one strip, so that the electrode edge positions are at  $c = d \exp(i\phi_n^{(\pm)})$  for  $\phi_n^{(\pm)}$  given by

$$\phi_n^{(+)} = \theta_0 - \frac{\theta_w}{2} + \frac{2\pi}{n} \{1, 2, \dots, n\}, \quad (20a)$$

$$\phi_n^{(-)} = \theta_0 + \frac{\theta_w}{2} + \frac{2\pi}{n} \{1, 2, \dots, n\}, \quad (20b)$$

as illustrated by Fig. 6.

Together, Eqs. (19) and (20) give the explicit position of the edges of strip electrodes to create an  $n$ th-order SE multipole guide at a distance  $d$  above the surface as illustrated in Fig. 7.

### C. Field of SE multipoles

To determine the analytical form of the field in an SE multipole guide described by Eq. (20), we will calculate the field in the corresponding cylinder configuration and then calculate the SE field through the map Eq. (18).

Firstly, we will determine the field of a strip electrode with edges at  $c_1, c_2$  in a cylinder with conducting walls. Calculating  $\Phi(p(c))$  with  $p_i = p(c_i)$  by Eq. (17) through the map Eq. (18), we find that when considering pairs of edges with opposite sign  $q_1 + q_2 = 0$ ,  $\Phi(c)$  is equivalent to the value obtained directly from Eq. (17) with  $z = c$  and  $z_i = c_i$ , as illustrated by Fig. 8. In other words, Eqs. (13), (16), and (17) for the field and potential of strip electrodes in an infinite grounded plane hold without any modification for the case of similar strip



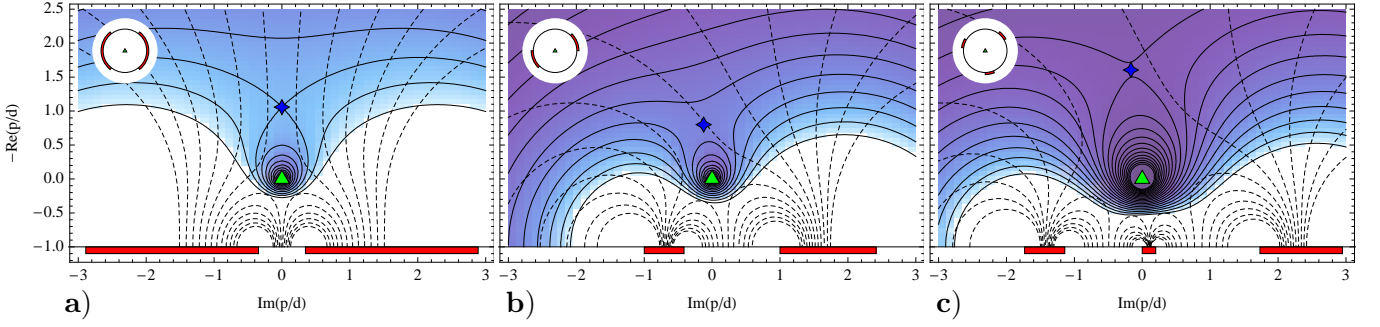


FIG. 7: (Color online) Examples of SE multipoles. Rectangles indicate rf electrode positions. Solid lines are contour lines of  $U_p$ , spaced by a factor of  $\sqrt{2}$ . The outermost line is at twice the maximal obtainable depth for quadrupole traps Eq. (30), corresponding to  $2 \times 55.8$  meV for the example parameters of Eq. (11). Dashed lines are field lines (some omitted). Insets show the electrode configuration in the cylinder representation. Triangle and star marks indicate the guide center and intrinsic saddle, respectively. In terms of the parametrization Eq. (20), the configurations are described by (a) the symmetric quadrupole ( $n = 2$ ) configuration ( $\theta_0 = \pi/2$ ) with  $\theta_w$  chosen for optimal intrinsic depth according to Eq. (28); (b) a tilted quadrupole configuration with  $\theta_w = \pi/4$  and  $\theta_0 = 5\pi/8$ ; and (c) an octupole ( $n = 3$ ) configuration with  $\theta_w = \pi/8$  and  $\theta_0 = \pi/16$ .

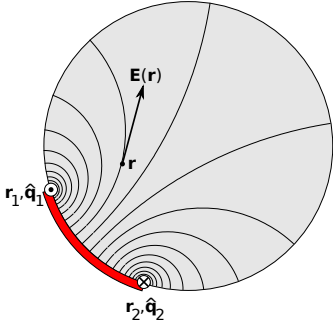


FIG. 8: (Color online) The electric field of the field of a strip electrode at potential  $V$  in a conducting cylinder has the exact same algebraic form as the field of a strip electrode in an infinite grounded plane, as given by Eq. (5).

electrodes on the walls of a grounded cylinder. This is in agreement with the fact that the field of an SE strip electrode meets the boundary conditions for a strip electrode in a conducting cylinder as illustrated by Fig. 4.

We can write the  $\phi_n^{(\pm)}$  values of the electrode edges Eq. (20) as  $\phi_n^{(0)} + \theta_0 \mp \theta_w/2$ , where  $\phi_n^{(0)} \equiv 2\pi\{1, 2, \dots, n\}/n$ . For  $\{c_i\} = d \exp(i\phi_n^{(0)})$  and  $q_i = 1$ , we find that the sum Eq. (17) can be completed since  $\prod_{k=1}^n (a - e^{i2\pi k/n}) = a^n - 1$ , and the corresponding (unphysical) single-sided complex potential is given by

$$\Phi_n^{(0)}(c) = V \frac{i}{\pi} \ln \left( \left( \frac{c}{d} \right)^N - 1 \right).$$

Since the positive and negative edge positions  $\phi_n^{(\pm)}$  can be obtained from  $\phi_n^{(0)}$  by rotations through an angle of  $\theta_0 \mp \theta_w$  around the origin, the combined potential  $\Phi_n(c)$  is equal to  $\Phi_n^{(0)}(c e^{-i(\theta_0 - \theta_w/2)}) - \Phi_n^{(0)}(c e^{-i(\theta_0 + \theta_w/2)})$ ,

which we write as

$$\Phi_n(c) \equiv V \frac{i}{\pi} \ln \left( \frac{(e^{-i(\theta_0 - \theta_w/2)} c)^n - d^n}{(e^{-i(\theta_0 + \theta_w/2)} c)^n - d^n} \right). \quad (21)$$

Equation (21) gives the exact form of a the complex potential of a cylinder multipole as parametrized by Eq. (20), and so together with the conformal map Eq. (18) give the potential for an SE multipole in the gapless plane approximation. The physical potential with the specified boundary conditions is  $\text{Re}\{\Phi_n[c(p(\mathbf{r}))]\} + Vn\theta_w/\pi$ .

To learn about the strength and orientation of the corresponding multipole field, we expand  $\partial\Phi_n(c)/\partial c$  to lowest order about the origin,

$$\frac{\partial\Phi_n}{\partial c} = e^{-in\theta_0} \frac{V}{d^n} \frac{2n}{\pi} \sin\left(\frac{n\theta_w}{2}\right) c^{n-1} + \mathcal{O}(c^{2n-1}). \quad (22)$$

Since by Eq. (18)  $dc/dp = 1/2$  at the origin, we have by Eq. (B7) that the lowest nonzero multipole coefficient of  $\Phi_n$  is

$$\alpha_p^{(n)} = 2^{-n} \frac{2}{\pi} \sin\left(\frac{n\theta_w}{2}\right) \frac{V}{d^n} e^{-in\theta_0}, \quad (23)$$

with  $\alpha_p^{(n)}$  as defined in Eq. (B6). The strength  $|\alpha_p^{(n)}|$  is seen to reach its maximal value of  $2V/\pi(2d)^n$  for  $\theta_w = \pi/n$ , corresponding to half the cylinder being covered with electrodes. The complex phase factor  $\exp(-in\theta_0)$  describes the orientation of the multipole.

At this point we can compare the strength of an SE multipole with that of a traditional (3D) multipole guide with the same ion-electrode distance. The strongest such guide is obtained when the electrodes are chosen as the  $\pm V/2$  equipotential surfaces of  $\text{Re}(z^n V/2d^n)$ , corresponding to a multipole coefficient of

$$\alpha_{3D}^{(n)} = \frac{1}{2} \frac{V}{d^n}, \quad (24)$$

so that the strongest possible SE multipole is a factor of  $2^n \pi/4$  weaker than the strongest possible 3D multipole of the same order and with the same ion-electrode distance.

For the case of quadrupole ( $n = 2$ ) guides employed in Paul traps, the strength of the rf field is usually parametrized by the dimensionless parameter  $q$  [10, 12, 14], which is related to the multipole expansion coefficients by

$$q \equiv \left| \alpha_p^{(2)} \right| \frac{4 Q}{M \Omega^2} = \frac{\sin(\theta_w)}{2\pi} q_0, \quad (25)$$

for  $q_0$  defined by Eq. (9). In the limit where the adiabatic approximation is valid, the corresponding secular frequency (in the absence of bias fields as discussed in Sec. VB), is well approximated by  $q\Omega/\sqrt{8}$  [12], corresponding to a maximal secular frequency of 5.5 MHz for the example parameters of Eq. (11). To compare the results presented here with experimental results, we note that Ref. [5] gives a measured value of  $q_{\text{exp}} = 0.54$  in the adiabatic approximation for an SE trap with  $\theta_w = \pi/4$ ,  $\theta_0 = \pi/4$ ,  $M = 24$  AMU,  $V_{\text{rf}} = 103$  V, and  $d = 40$   $\mu\text{m}$ . This is in good agreement with the value  $q = 0.55$  predicted by Eq. (25).

## V. DEPTH OF SE MULTIPOLE TRAPS

In this section we will investigate the potential depth that can be obtained when using SE multipoles for rf traps. As in Sec. III on the SE ring trap, we will assume the adiabatic approximation Eq. (2) to be valid. In Sec. VA, we will consider the intrinsic depth, i.e., the depth in the absence of control fields. Here we will mostly work with crude estimates, while Appendix A provides a derivation of some exact results. In Sec. VB we consider the effects of control fields on the total potential depth provided by  $U_{\text{eff}}$ .

Our current understanding of SE multipole depth is far from complete and, in particular, Sec. VA contains results based on conjectures as detailed in Appendix A.

### A. Intrinsic depth

In terms of the complex rf potential  $\Phi_{\text{rf}}$  the ponderomotive potential is proportional to  $|\Phi'_{\text{rf}}|^2$  where we use a prime to denote differentiation with respect to  $p$ . It follows that a necessary condition for an intrinsic saddle point is that  $\Phi'_{\text{rf}} \Phi''_{\text{rf}} = 0$ . Since the zeros of  $\Phi'_{\text{rf}}$  are not saddles, the saddle point  $p_s$  must fulfill  $\Phi''_{\text{rf}}(p_s) = 0$ .

For the multipole configuration described by the complex potential  $\Phi_n$ , we can take advantage of the fact that the expansion  $\Phi_n \approx \alpha_c^{(n)} c^n$  by Eq. (21) is good to order  $2n - 1$  to establish a reasonable estimate of the saddle point  $p_s^{(n)}$  fulfilling  $\Phi''_n(p_s^{(n)}) = 0$ . By the chain rule

$$\Phi'' \equiv \frac{\partial^2 \Phi}{\partial p^2} = \left( \frac{\partial^2 \Phi}{\partial c^2} - \frac{\partial \Phi}{\partial c} \frac{\partial^2 p}{\partial c^2} / \frac{\partial p}{\partial c} \right) \left( \frac{\partial p}{\partial c} \right)^{-2},$$

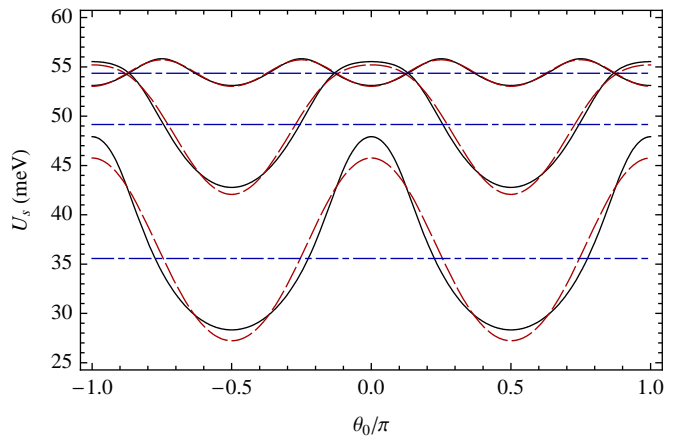


FIG. 9: (Color online) Intrinsic depth of quadrupoles ( $n = 2$ ) as a function of  $\theta_0$  for  $\theta_w/\pi$  equal to 0.3, 0.4, and 0.5 with the parametrization described by Eq. (20) for the example parameters of Eq. (11). The depth scales as  $U_0$  (Eq. (12)). Solid lines are exact results, corresponding to cuts of the contour plot shown in Fig. 10. Dashed lines correspond to evaluating the exact field at the simplest saddle-point estimate  $p_s^{(2,0)}$  of Eq. (26). Higher-order approximation as given by Eq. (A3a), could not be discerned from the exact results. Dash-dotted lines show the value of the crude estimate of Eq. (27).

so that for  $\Phi \propto c^n$  we have a saddle at  $c = d(1-n)/(1+n)$  corresponding to  $p = d(1-n)$ , which we take to be a reasonable estimate of  $p_s^{(n)}$  as follows:

$$p_s^{(n)} \approx p_s^{(n,0)} \equiv d(-n+1). \quad (26)$$

The saddle point of  $U_p$  for  $\Phi_n$  is consequently located approximately above the center of the guide at a distance of  $n$  times the ion-electrode distance from the electrode plane. An iterative procedure for obtaining better estimates  $p_s^{(n,k)}$ ,  $k = 1, 2, \dots$  of the true saddle  $p_s^{(n)}$  is given by Eq. (A3a).

As illustrated by Fig. 9,  $U_p(p_s^{(n,0)})$  is a reasonable estimate of the intrinsic depth  $U_s^{(n)} \equiv U_p(p_s^{(n)})$  corresponding to  $\Phi_n$ . While  $U_p$  can be evaluated exactly according to Eq. (21) by Eq. (A1), the expression is somewhat involved. A crude estimate of  $U_s^{(n)}$  can be obtained by employing the approximation  $\Phi_n(p) \approx \alpha_c^{(n)} c(p)^n$  again to estimate the  $\Phi'(p_s^{(n,0)})$ , resulting in

$$U_s^{(n)} \equiv U_0 \left| \frac{\Phi'_n(p_s^{(n)})}{V/d} \right|^2 \approx \left[ \frac{1}{n} \sin\left(\frac{n\theta_w}{2}\right) \frac{4}{e^2\pi} \right]^2 U_0, \quad (27)$$

which for the example parameters of Eq. (11) corresponds to  $U_s^{(n)} \approx n^{-2} \sin^2(n\theta_w/2) 180$  meV. The value of the crude estimate is illustrated in Fig. 9.

A more detailed analysis of the intrinsic depth is carried out in Appendix A. The main conclusion is that for any value of  $n$  there is a special saddle position  $\bar{p}_s^{(n)}$  and



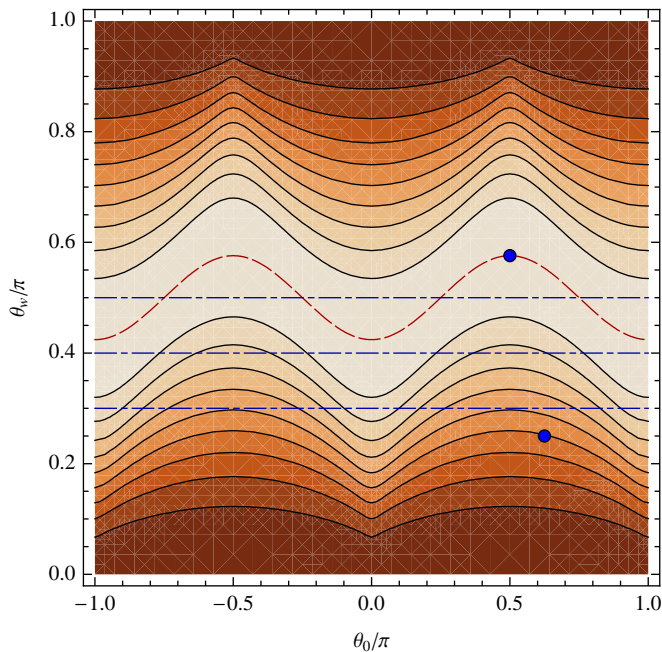


FIG. 10: (Color online) Contour plot showing the intrinsic depth  $U_s^{(n)}$  of quadrupole ( $n = 2$ ) guides as a function of the parameters  $\theta_0$  and  $\theta_w$  appearing in Eq. (20). Contour lines are spaced by 0.1 times the maximal quadrupole depth  $\bar{U}_s^{(2)}$  given by Eq. (30). The dashed line indicates points where Eq. (28) holds. For these points the maximal depth  $U_s^{(n)} = \bar{U}_s^{(n)}$  is obtained. The symmetries of the depth are discussed in Appendix A, and the dash-dotted lines (dots) indicate parameter values also illustrated in Fig. 9 [Figs. 7(a) and 7(b)].

a real-valued constant  $A_n$ , both independent of the parameters  $\theta_0$  and  $\theta_w$ , so that  $p_s^{(n)} = \bar{p}_s^{(n)}$  if and only if  $\theta_w$  and  $\theta_0$  fulfill

$$\cos(n\theta_w/2) = A_n \cos(n\theta_0). \quad (28)$$

Further, the intrinsic depth is the same for all combinations of  $\theta_0$  and  $\theta_w$  fulfilling this requirement, and this depth is the maximum obtainable in an  $n$ th-order SE multipole. To obtain the maximal depth  $\bar{U}_s^{(n)} \equiv U_s^{(n)}(\bar{p}_s^{(n)})$  and maximal strength simultaneously, we must, by Eq. (23), have  $\theta_w = \pi/n$ , so that according to Eq. (28),  $\cos(n\theta_0)$  must also vanish. This corresponds to an antisymmetrical configuration where a reflection in the real axis ( $z$  axis) map rf electrodes to ground electrodes and vice versa.

For quadrupoles ( $n = 2$ ),  $A_2 = \sqrt{5} - 2$  and the special saddle is located at

$$\bar{p}_s^{(2)} = -d \left( \sqrt{2 + \sqrt{5}} - 1 \right). \quad (29)$$

The maximal intrinsic depth of a quadrupole trap is

$$\bar{U}_s^{(2)} \equiv \frac{5\sqrt{5} - 11}{2\pi^2} U_0, \quad (30)$$

with  $U_0$  given by Eq. (12). For the example parameters of Eq. (11)  $\bar{U}_s^{(2)} = 55.8$  meV. In the quadrupole case, the antisymmetric configuration ( $\theta_0 = \pi/2$ ,  $\theta_w = \pi/2$ ) achieving maximal depth and strength simultaneously is referred to as the four-wire trap [4, 5].

## B. Depth in the presence of static fields

The remainder of the section is devoted to a brief description of the impact on static control fields on trap depth. For simplicity, we will not consider the effect of a confining potential along the axis of translational symmetry. Also, we only consider fields that vanish at the trap center, since any field at this point would shift the trapping minimum of  $U_{\text{eff}}$  to a region of nonzero rf amplitude leading to micromotion.

By applying different control voltages to different electrodes, a control field of this type can be implemented with almost any set of two or more electrodes. Here, we will only consider the possibility of applying a bias voltage  $V_{c,\text{rf}}$  to the rf electrodes. In practical applications, this approach has the advantage that a control field generated by the rf electrodes is guaranteed to have a field zero exactly at the trap center, even when departures from the idealized gapless plane geometry are taken into account. Also, this approach ensures that the principal axes of the control and rf quadrupoles are aligned, allowing an analytical solution for the motion of a trapped ion valid outside the adiabatic approximation [14]. The main practical obstacle to applying a bias to the rf field is that it is incompatible with grounding part of the rf resonator.

For a bias voltage  $V_{c,\text{rf}}$  applied to the rf electrodes, the combined effective potential is equal to

$$U_{\text{eff}}(\mathbf{r}) = U_0 \left( v_c \Theta_{\text{rf}}(\mathbf{r}) + d^2 |\nabla \Theta_{\text{rf}}(\mathbf{r})|^2 \right), \quad (31)$$

where  $\Theta_{\text{rf}}(\mathbf{r}) = \bar{V}_{\text{rf}}(\mathbf{r})/V_{\text{rf}}$  is the rf electrode basis function and

$$v_c \equiv \frac{Q V_{c,\text{rf}}}{U_0}, \quad (32)$$

parametrizes the strength of the bias field. The ratio of the modified to the intrinsic depth only depends on  $v_c$ , so that the relative improvement of trap depth, which can be achieved by biasing, is a purely geometrical factor and does not depend on the operating parameters of the trap.

An important consideration when applying a control field is the effect on trap stability. For the quadrupole trap with a control field applied as a bias to the rf electrode, the stability criteria can be established analytically [10, 14]. For this purpose, the bias strength is parametrized by the dimensionless parameter  $a = 2q V_{c,\text{rf}}/V_{\text{rf}}$  together with  $q$  as defined by Eq. (25). The stable region usually used for QIP ion traps includes

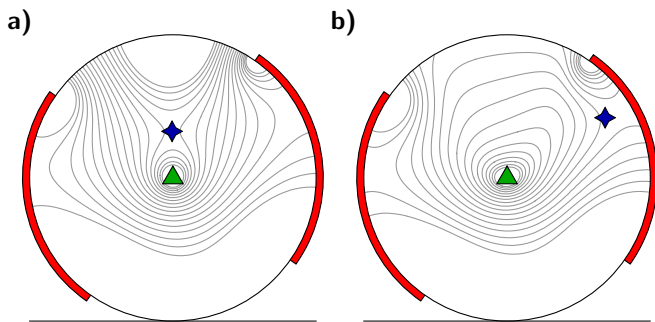


FIG. 11: (Color online) Contour plot of  $U_{\text{eff}}$  for the unbiased (a) and optimally biased (b) quadrupole configuration with  $\theta_0 = 100^\circ$  and  $\theta_w = \pi/2$ . In order to illustrate the potential in the full trapping region, the potential has been mapped to the  $c$  plane so that what is plotted is  $U_{\text{eff}}(p(c))$  with  $p(c)$  given by Eq. (18). Contours are spaced by a factor of  $\sqrt{2}$  from  $\bar{U}_s^{(2)}/4$  to  $64\bar{U}_s^{(2)}$  with  $\bar{U}_s^{(2)}$  as defined in Eq. (30). Stars indicate the lowest saddle points, and triangles indicate the trap centers. As discussed in the text, the relative increase in depth by a factor of 9.8 is independent of operating parameters.

$(a, q)$  for which  $q < 0.7$  and  $|a/q^2| < 0.5$  [10, 14], where the second constraint is the one of interest here. If we introduce the dimensionless “geometrical” quadrupole strength  $\bar{\alpha}^{(2)} \equiv \alpha^{(2)}d^2/V$ , so that  $q = |\bar{\alpha}^{(2)}|q_0$ , we have that  $a/q^2 = v_c/8|\bar{\alpha}^{(2)}|$  so that the stability requirement is a geometrical property independent of the operating parameters. For the parametrization of Eq. (20) we have by Eq. (23) that  $|\bar{\alpha}^{(2)}| = \sin(\theta_w)/2\pi$  so that the stability criterion is well approximated by  $|v_c| \lesssim 0.6 \sin(\theta_w)$ .

As an example, we consider a quadrupole guide ( $n = 2$ ) with parameters  $\theta_0 = 100^\circ$ , and  $\theta_w = \pi/2$ . Here we find numerically that a maximum depth of  $9.8\bar{U}_s^{(2)}$  is obtained for  $v_c = 0.18$ , corresponding to  $a/q^2 = 0.14$ , well inside the stable region described above. The form of the optimally biased  $U_{\text{eff}}$  is illustrated by Fig. 11. For the example parameters of Eq. (11), the optimal bias voltage is  $V_{c,\text{rf}} = v_c U_0/Q = 1.1 \text{ V}$ . Note that although the optimal bias voltage is dependent on operating parameters, the ratio  $a/q^2$  at optimal bias is constant, and so the optimally biased configuration will always be stable, provided it meets the constraint  $q < 0.7$  corresponding to a lower bound on  $\Omega$ .

## VI. CONCLUSION AND OUTLOOK

In conclusion, we have obtained a wide range of analytical results on SE traps. The most significant are the explicit parametrization of SE multipole geometry as given by Eq. (19), together with the results on the exact field [Eq. (21)], strength [Eq. (23)], and intrinsic depth [Eq. (30), Figs. 9 and 10].

There are, however, a number of open questions relating to SE traps.

In direct continuation of the work presented here it

would be of interest to establish a formal proof that the intrinsic multipole depth is maximal exactly when the saddle is located on the special saddle point as conjectured in Appendix A. Also, the adiabatic approximation will in many cases be invalid within the stable region suggested by the intrinsic depth. It would consequently be of interest to study the depth beyond the adiabatic approximation [25].

The limitations of the gapless plane approximation used throughout this paper should be quantified in two respects. Least importantly, the effect of finite gaps between electrodes are of interest because increasing the gap size decreases field gradients and the capacitive load of the trap. More important are finite-size effects: In a realistic implementation there will be grounded surfaces within a few cm of the electrode surface. Finite-size corrections will be first order in the total electrode extend relative to this distance, and could consequently be significant.

Finally, limitations on the possible global structure of SE fields are not fully understood. In spite of recent progress on the possible structure of intersections for rf trap networks [11], it is not clear whether it is possible to implement ideal intersections in SE traps. Also, arrays of SE traps are being studied in several contexts [21, 26].

## Acknowledgments

The author gratefully acknowledges discussions with Jason Amini, Dietrich Leibfried, and David Wineland. This work was supported by the Danish National Research Agency, the Carlsberg Foundation, and the QIP IRC (Grant No. GR/S82176/01).

## APPENDIX A: SADDLES IN MULTIPOLE GUIDES

This appendix is devoted to a detailed discussion of the exact intrinsic depth and saddle position in SE multipole guides. We use the term “intrinsic saddle point” to refer to a saddle point of the ponderomotive part of  $U_{\text{eff}}$  as given by Eq. (2). As discussed in Sec. V A, such saddle points must be located at zeros of  $\Phi_{\text{rf}}''$ . The following is devoted to identifying such zeros for  $\Phi_{\text{rf}}$  given by the exact multipole potential  $\Phi_n$  of Eq. (1). To make the algebra more manageable, we will set  $V$  and  $d$  to unity, and introduce a new complex coordinate system with its origin in the electrode plane.

$$u \equiv \frac{p}{d} - 1.$$

With these conventions,  $\Phi'_n = (\partial\Phi_n/\partial c)/(\partial u/\partial c)$  can be given a compact form in terms of  $c$  and  $\tilde{c} = e^{-i\theta_0}c$ .

$$\Phi'_n = \frac{n}{\pi} \frac{\sin(n\theta_w/2)}{\tilde{c}^n - 2\cos(n\theta_w/2) + \tilde{c}^{-n}} \frac{(1+c)^2}{c}. \quad (\text{A1})$$

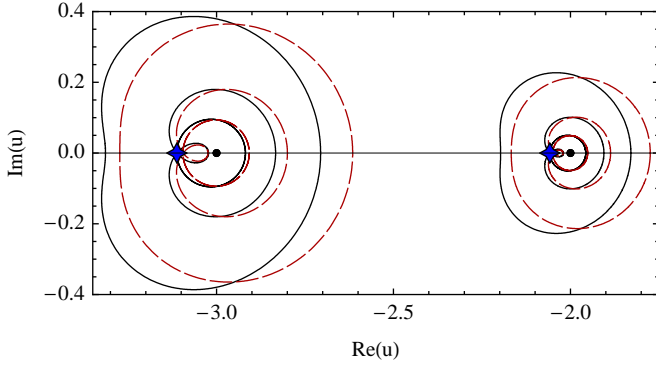


FIG. 12: (Color online) Orbits of the intrinsic saddle position for  $n = 2$  and  $3$  as a  $\theta_0$  is varied for  $n\theta_w/\pi = 0.7, 0.9$ , and  $1$ . Solid (dashed) lines show the exact value (the estimate  $u_s^{(n,1)}$ ) of  $u_s^{(n)}$ . Dots show the crude estimates  $u_s^{(n,0)} = -n$ . Note that when  $\theta_w$  is too large to be compatible with Eq. (A4) for any value of  $\theta_0$ , the orbits do not pass through the special saddle positions  $\bar{u}_s^{(n)}$  (stars).

In terms of  $u$ , we have that  $c = (1+u)/(1-u)$  so that

$$\Phi'_n = \frac{4n}{\pi} \sin\left(\frac{n\theta_w}{2}\right) \frac{(1-u^2)^{n-1}}{P(u)},$$

where the polynomial  $P(u) \equiv P_+(u) + iP_-(u)$  is described as a sum of even and odd parts,  $P_{\pm}$ , given by

$$P_+(u) \equiv \cos(n\theta_0) [(1-u)^{2n} + (1+u)^{2n}] - 2(1-u^2)^n \cos\left(\frac{n\theta_w}{2}\right), \quad (\text{A2a})$$

$$P_-(u) \equiv \sin(n\theta_0) [(1-u)^{2n} - (1+u)^{2n}]. \quad (\text{A2b})$$

We see that  $\Phi'_n$  has zeros of order  $n-1$  at  $u = \pm 1$ , corresponding to the multipole center and its mirror image in the electrode plane. Also, there are  $2n$  first-order poles at the roots of  $P$ , which are located at the electrode edges on the imaginary axis.

To establish the saddle positions, we differentiate  $\Phi'_n$  again, and write the derivative as

$$\Phi''_n = -\Phi'_n \frac{1}{P(u)(1-u^2)} S(u),$$

where  $S(u) \equiv S_+(u) + iS_-(u)$  is a polynomial of order  $2n+1$  with even or odd parts given by

$$S_{\pm}(u) = 2u(n-1)P_{\pm}(u) + (1-u^2)P'_{\pm}(u),$$

so that, in particular,

$$S_-(u) = -2\sin(n\theta_0) \left( u [(u-1)^{2n} - (u+1)^{2n}] + n [(u-1)^{2n} + (u+1)^{2n}] \right).$$

We see that  $\Phi''_n$  has zeros of order  $n-2$  at  $u = \pm 1$  and second-order poles at the electrode edges, while the  $2n+1$  roots of  $S$  describe the possible saddle positions.

To determine the root structure for  $S$ , we note the following: According to the edge-current picture, the field must be antisymmetric under inversion in the electrode plane so that  $\Phi'(u)^* = \Phi'(-u^*)$ . This implies that  $\Phi'$  is real on the imaginary axis, or equivalently, that the electrode field is perpendicular to the electrodes at the surface as it should be. Since  $\Phi'$  will diverge with equal sign at the two sides of an electrode or ground strip, there must be a zero of  $\Phi''$  on each such segment on the imaginary axis. Further, since these zeros must also be roots of  $S(u)$ , there will be a zero of  $S$  between each of the  $2n$  edges for a total of  $2n-1$  zeros on the electrode plane, i.e., the imaginary axis. As  $S(u)$  is a polynomial of order  $2n+1$  this leaves two roots outside the electrode plane, which we identify as the saddle interest to us, which we will denote  $u_s^{(n)}$  and for which  $\text{Re}(u_s^{(n)}) < 0$ , and its mirror image  $-(u_s^{(n)})^*$ .

It follows from the above discussion that the saddle position  $u_s^{(n)}$  corresponding to  $\Phi_n$  as given by Eq. (21) is the unique root of  $S(u) = 0$  with  $\text{Re}(u) < 0$ . The roots of  $S$  can be calculated numerically by standard techniques, allowing a simple procedure for determining the intrinsic saddle points for any multipole. Alternatively, the following heuristic iterative procedure

$$u_s^{(n,0)} = -n, \quad (\text{A3a})$$

$$u_s^{(n,k+1)} = n u_s^{(n,k)} + \frac{1-u^2}{2} \frac{P'(u)}{P(u)}, \quad (\text{A3b})$$

found by solving  $S(u) = 0$  for the first order  $u$ , has been observed to converge relatively quickly to the main saddle as illustrated in Fig. 12. In particular, for estimating the trap depth, the zeroth- or first-order estimates established by evaluating  $\Phi'_n$  at  $u_s^{(n,0)}$  or  $u_s^{(n,1)}$  are mostly sufficient, as illustrated in Fig. 9. The initial estimate  $u_s^{(n,0)}$  is that identified in Sec. V A, but we note that it could also be obtained by starting the iteration at the trap center,  $u = -1$ .

### 1. Saddle on the real axis

It turns out that configurations where the saddle is on the real axis, i.e., directly above the trap center, have a special significance.

There are two types of symmetry that will guarantee the saddle to be on the real axis. Firstly, when  $\theta_0$  is equal to an integer multiple of  $\pi/n$ , the electrode configuration is symmetric under reflection in the real axis, ensuring that the saddle must be located on the axis. In this symmetric configuration,  $S_-(u)$  is identically zero so that  $S = S_+$ . A less obvious symmetry is found when  $\theta_w = \pi/n$  and  $\theta_0$  is an odd multiple of  $\pi/2n$ , so that the electrode structure is antisymmetric under reflection in the real axis, i.e., rf electrodes are mapped to grounded areas and vice versa. Since the ponderomotive potential only depends on the field strength, this symmetry

TABLE I: Numerical values of the special saddle point  $\bar{u}_s^{(n)}$  and the factor  $A_n$  appearing in Eq. (A4), describing the relation between  $\theta_0$  and  $\theta_w$  for optimal depth. Exact values for  $n = 2$  are given by Eq. (29).

$n$	$-\bar{u}_s^{(n)}/n$	$A_n$
2	1.02909	0.236068
3	1.03742	-0.266149
4	1.04044	0.276076
10	1.04375	0.286475
20	1.04422	0.287935
50	1.04436	0.288342
100	1.04438	0.288400
200	1.04438	0.288415

will also conserve the saddle which must consequently be located on the real axis.

The antisymmetric configuration turns out to be of special interest, and we will refer to the saddle position in this case as  $\bar{u}_s^{(n)}$ .  $\bar{u}_s^{(n)}$  can be calculated as the negative real root of  $S_-$ , since in the antisymmetric configuration  $\cos(n\theta_0)$  and  $\cos(n\theta_w/2)$  both vanish so that  $S = iS_-$ .

Although we have introduced  $\bar{u}_s^{(n)}$  as the saddle position for the anti-symmetric configuration, so that in particular  $\bar{u}_s^{(n)}$  is independent of  $\theta_0$  and  $\theta_w$ , it turns out that there is a number of configurations with the same saddle position, and that these have very interesting properties. Firstly, we note that since  $P_+$  and thus  $S_+$  depends on  $\theta_0$  and  $\theta_w$  only through the ratio of  $\cos(n\theta_w/2)$  to  $\cos(n\theta_0)$ , there will for any value of  $n$  be a constant  $A_n$  so that  $S_+(\bar{u}_s^{(n)}) = 0$  whenever

$$\cos(n\theta_w/2) = A_n \cos(n\theta_0). \quad (\text{A4})$$

Since the roots of  $S_-$  are independent of  $\theta_0$  and  $\theta_w$  it follows that when the condition of Eq. (A4) is met, the special saddle  $\bar{u}_s^{(n)}$  will be a root both of  $S_+$  and  $S_-$ . Since  $S = S_+ + iS_-$  it follows that  $\bar{u}_s^{(n)}$  will also be a root of  $S$  and consequently be the actual saddle position through an ‘‘accidental’’ symmetry as illustrated in Fig. 12. We have not been able to obtain closed expressions for  $\bar{u}_s^{(n)}$  for  $n > 2$ , but give numerical values in Table I.

The key property of the special saddle point is that all configurations which fulfill Eq. (A4), and thus have the saddle at  $\bar{u}_s^{(n)}$ , obtain the maximal intrinsic depth possible for a SE multipole of order  $n$ .

$$U_s^{(n)}(\theta_w, \theta_0) = \bar{U}_s^{(n)} \Leftrightarrow u_s^{(n)}(\theta_w, \theta_0) = \bar{u}_s^{(n)}.$$

This result has only been proven for  $n = 2$  but we conjecture it to be true for all  $n$  based on numerical results.

## APPENDIX B: 2D ELECTROSTATICS

This section recapitulates a number of results on 2D electrostatics.

### 1. Pólya field

The Pólya field gives a one-to-one mapping from 2D electrostatic fields to analytical functions on the complex plane [27]. We consider the canonical mapping  $(x, y) \mapsto z \equiv x + iy$  from  $\mathbb{R}^2$  to  $\mathbb{C}$  and map the electrical field  $\mathbf{E}(x, y)$  to the complex-valued function

$$\tilde{E}(x + iy) \equiv E_x(x, y) + iE_y(x, y). \quad (\text{B1})$$

Note that  $\tilde{E}$  is not related to the complex amplitude used in electrodynamics to describe phase relations.

We will consider  $z \equiv x + iy$  and  $\bar{z} \equiv x - iy$  to be independent variables with respect to differentiation, so that  $\partial_z \equiv \frac{1}{2}\partial_x - i\frac{1}{2}\partial_y$  and  $\partial_{\bar{z}} \equiv \frac{1}{2}\partial_x + i\frac{1}{2}\partial_y$  are the Wirtinger derivatives often used in physics. With this convention we find that

$$\frac{\partial \tilde{E}}{\partial z} = \frac{\partial \tilde{E}^*}{\partial \bar{z}} = \frac{1}{2}(\nabla \cdot \mathbf{E} + i\hat{z} \cdot \nabla \times \mathbf{E}), \quad (\text{B2})$$

so that  $\nabla \cdot \mathbf{E}$  and  $\nabla \times \mathbf{E}$  vanish, as they must for an electrostatic field in free space, if and only if  $\partial \tilde{E}/\partial z = 0$ . In terms of the Wirtinger derivatives, a complex function  $f(z)$  is differentiable if and only if  $\partial f(z)/\partial \bar{z} = 0$ , and Eq. (B2) consequently implies that  $\mathbf{E}$  is a free space electrostatic field if and only if  $\tilde{E}^*$  is complex differentiable and thus analytic. In complex analysis, the field  $\mathbf{E}$  is known as the Pólya field of  $E^*$ .

In terms of the real-valued potential  $V$  the analytical function  $\tilde{E}^*$  is seen to be given by

$$\tilde{E}^* = -\left(\frac{\partial V}{\partial x} - i\frac{\partial V}{\partial y}\right) = -2\frac{\partial V}{\partial z}. \quad (\text{B3})$$

Note that since  $V$  is real it is not analytic and especially not an antiderivative of  $-\tilde{E}^*/2$ . On the other hand, the analytic function  $-\tilde{E}^*$  has an analytic antiderivative  $\Phi(z)$ , so that

$$\tilde{E}^* = -\frac{\partial \Phi}{\partial z}, \text{ and } \frac{\partial \Phi}{\partial \bar{z}} = 0. \quad (\text{B4})$$

The antiderivative is unique up to the addition of a complex constant. By inspection, we see that  $V$  defined as  $V(x, y) = \text{Re}(\Phi(x + iy))$  does fulfill Eq. (B3). The imaginary part of  $\Phi$  is known as the harmonic conjugate of  $V$ , and we note that since  $\nabla \text{Im}(\Phi) \cdot \mathbf{E} = 0$ , lines of constant  $\text{Im}(\Phi)$  are field lines of  $\mathbf{E}$ .

### 2. Conformal maps

In two dimensions, conformal, or angle-preserving, maps will map a solution of the Laplace equation to another solution of the Laplace equation in the sense that if  $\nabla^2 V(\mathbf{r}) = 0$  and  $M(\mathbf{r})$  is a conformal map, then we find that  $\nabla^2 V(M(\mathbf{r})) = 0$ . In the complex plane a map  $w \mapsto z(w)$  is conformal if and only if the function  $z(w)$  is

analytic. If  $\tilde{E}(z)$  is a divergence-free and irrotational field, so that  $\tilde{E}^*(z) = -\partial\Phi(z)/\partial z$  for some complex-valued analytic potential  $\Phi(z)$  and  $z = z(w)$  is an analytical function,  $\Phi_w(w) \equiv \Phi(z(w))$  is also analytic so that by Eq. (B2) the Pólya field of

$$\tilde{E}_w^*(w) \equiv -\frac{\partial\Phi_w(w)}{\partial w} = \tilde{E}^*(z(w))\frac{\partial z(w)}{\partial w}, \quad (\text{B5})$$

is indeed divergence-free and irrotational by the results of the last section.

### 3. 2D multipole expansion

In two dimensions, a naive specification of the  $n$ th multipole moment of a harmonic potential  $V$  would involve the  $n + 1$  distinct partial derivatives of order  $n$ . Considering the constraints imposed by the Laplace condition would, however, leave only two free parameters. Working in the complex notation, this result is obvious, as the

multipole expansion of  $V$  is nothing more than the series expansion of a corresponding analytical potential  $\Phi$  so that  $V = \text{Re}(\Phi)$ . We will write the multipole expansion around the origin as

$$\Phi(z) = \sum_{n=0}^{\infty} \alpha^{(n)} z^n. \quad (\text{B6})$$

We will now consider the mapping of the multipole strengths: If  $\Phi(z) = \alpha^{(n)} z^n + \mathcal{O}(z^{n+1})$  and  $\Phi_w(w) \equiv \Phi(z(w))$ , where  $z = z(w)$  is a conformal map so that  $z(0) = 0$ , we see that  $\Phi_w(w) = \alpha^{(n)} (\partial z/\partial w)^n w^n + \mathcal{O}(w^{n+1})$  so that the lowest-order multipole moment of  $\Phi_w$  is

$$\alpha_w^{(n)} = \alpha^{(n)} \left( \frac{\partial z}{\partial w} \right)^n, \quad (\text{B7})$$

where  $\partial z/\partial w$  is evaluated at the origin.

- 
- [1] D. Kielpinski, C. Monroe, and D. J. Wineland, “Architecture for a large-scale ion-trap quantum computer,” *Nature* **417** (2002) 709.
- [2] D. Leibfried, E. Knill, C. Ospelkaus, and D. J. Wineland, “Transport quantum logic gates for trapped ions,” *Phys. Rev. A* **76** (2007) 032324.
- [3] C. Ospelkaus, C. E. Langer, J. M. Amini, K. R. Brown, D. Leibfried, and D. J. Wineland, “Trapped-ion quantum logic gates based on oscillating magnetic fields,” *Phys. Rev. Lett.* **101** (2008) 090502, [arXiv:0805.2165](#).
- [4] J. Chiaverini, R. B. Blakestad, J. Britton, J. D. Jost, C. Langer, D. Leibfried, R. Ozeri, and D. J. Wineland, “Surface-electrode architecture for ion-trap quantum information processing,” *Quantum Inf. Comput.* **5** (2005) 419.
- [5] S. Seidelin, J. Chiaverini, R. Reichle, J. J. Bollinger, D. Leibfried, J. Britton, J. H. Wesenberg, R. B. Blakestad, R. J. Epstein, D. B. Hume, J. D. Jost, C. Langer, R. Ozeri, N. Shiga, and D. J. Wineland, “A microfabricated surface-electrode ion trap for scalable quantum information processing,” *Phys. Rev. Lett.* **96** (2006) 253003, [arXiv:quant-ph/0601173](#).
- [6] J. Labaziewicz, Y. Ge, P. Antohi, D. Leibbrandt, K. R. Brown, and I. L. Chuang, “Suppression of heating rates in cryogenic surface-electrode ion traps,” *Phys. Rev. Lett.* **100** (2008) 013001.
- [7] Q. A. Turchette, D. Kielpinski, B. E. King, D. Leibfried, D. M. Meekhof, C. J. Myatt, M. A. Rowe, C. A. Sackett, C. S. Wood, W. M. Itano, C. Monroe, and D. J. Wineland, “Heating of trapped ions from the quantum ground state,” *Phys. Rev. A* **61** (2000) 063418.
- [8] R. J. Epstein, S. Seidelin, D. Leibfried, J. H. Wesenberg, J. J. Bollinger, J. M. Amini, R. B. Blakestad, J. Britton, J. P. Home, W. M. Itano, J. D. Jost, E. Knill, C. Langer, R. Ozeri, N. Shiga, and D. J. Wineland, “Simplified motional heating rate measurements of trapped ions,” *Phys. Rev. A* **76** (2007) 033411, [arXiv:0707.1528](#).
- [9] R. Reichle *et al.*, “Networking Surface Electrode Ion Traps for Large-Scale QIP.” Poster at NIST workshop on trapped ion quantum computing, 2006. <http://tf.nist.gov/ion/workshop2006/t01.pdf>.
- [10] W. Paul, “Electromagnetic traps for charged and neutral particles,” *Rev. Mod. Phys.* **62** (1990) 531–540.
- [11] J. H. Wesenberg, “Intersecting paths of zero field in irrotational and divergence-free vector fields,” [arXiv:0802.3162](#). To appear in *Phys. Rev. A*.
- [12] D. J. Wineland, C. R. Monroe, W. M. Itano, D. Leibfried, B. E. King, and D. Meekhof, “Experimental issues in coherent quantum-state manipulation of trapped atomic ions,” *J. Res. Natl. Inst. Stand. Technol.* **103** (1998) 259.
- [13] D. Hucul, M. Yeo, W. K. Hensinger, J. Rabchuk, S. Olmschenk, and C. Monroe, “On the transport of atomic ions in linear and multidimensional ion trap arrays,” *Quantum Inf. Comput.* **8** (2008) 0501–0578, [arXiv:quant-ph/0702175](#).
- [14] P. K. Ghosh, *Ion Traps*. Clarendon Press, Oxford, 1995.
- [15] H. G. Dehmelt, “Radiofrequency spectroscopy of stored ions i: Storage,” *Adv. At. Mol. Phys.* **3** (1967) 53.
- [16] M. H. Oliveira and J. A. Miranda, “Biot-Savart-like law in electrostatics,” *Eur. J. Phys.* **22** (2001) 31, [arXiv:physics/0011015](#).
- [17] R. Folman, P. Krüger, D. Cassettari, B. Hessmo, T. Maier, and J. Schmiedmayer, “Controlling cold atoms using nanofabricated surfaces: Atom chips,” *Phys. Rev. Lett.* **84** (2000) 4749–4752.
- [18] W. Hansel, P. Hommelhoff, T. W. Hänsch, and J. Reichel, “Bose-Einstein condensation on a microelectronic chip,” *Nature* **413** (2001) 498–501.
- [19] R. Folman, P. Krüger, J. Schmiedmayer, J. Denschlag, and C. Henkel, “Microscopic atom optics: From wires to an atom chip,” *Adv. At., Mol., Opt. Phys.* **48** (2002)



- 263–356, [arXiv:0805.2613](#).
- [20] J. D. Hanson and S. P. Hirshman, “Compact expressions for the Biot-Savart fields of a filamentary segment,” *Phys. Plasmas* **9** (2002) 4410.
  - [21] J. Chiaverini and W. E. Lybarger, Jr., “Laserless trapped-ion quantum simulations without spontaneous scattering using microtrap arrays,” *Phys. Rev. A* **77** (2008) 022324, [arXiv:0711.0233](#).
  - [22] R. Schmied. Private communication, 2008.
  - [23] S. Tryka, “A method for calculating the average solid angle subtended by a circular disk from uniformly distributed points within a coaxial circular plane,” *Rev. Sci. Instrum.* **70** (1999) 3915.
  - [24] G. Birkhoff and S. Mac Lane, *A Survey of Modern Algebra*. AK Peters, Ltd., Wellesley, 1997.
  - [25] J. Mikosch, U. Fruhling, S. Trippel, D. Schwalm, M. Weidemuller, and R. Wester, “Evaporation of buffer-gas-thermalized anions out of a multipole rf ion trap,” *Phys. Rev. Lett.* **98** (2007) 223001.
  - [26] R. Schmied, T. Roscilde, V. Murg, D. Porras, and J. I. Cirac, “Quantum phases of trapped ions in an optical lattice,” *New J. Phys.* **10** (2008) 045017, [arXiv:0712.4073](#).
  - [27] G. Pólya and G. Latta, *Complex Variables*. John Wiley & Sons, New York, 1974.